

Estimating tidal deformability, moment of inertia, quadrupole moment of merger components of GW170817

Sajad A. Bhat and Debades Bandyopadhyay
*Astroparticle Physics and Cosmology Division,
Saha Institute of Nuclear Physics, 1/AF Bidhannagar,
Kolkata-700064, India and Homi Bhabha National Institute,
Training School Complex, Anushaktinagar, Mumbai-400094*

Abstract

Tidal deformability, moment of inertia and quadrupole moment of merger components of GW170817 are investigated using different equations of state (EoSs) involving nucleons, Λ hyperons, quarks resulting in $2M_{\odot}$ neutron stars. This calculation is performed for low spin case. It is found from the computations of tidal deformability parameters that soft to moderately stiff equations of state are allowed by the 50% and 90% credible regions obtained from the gravitational wave observation of binary neutron star merger GW170817, whereas the stiffest hadron-quark EoSs which lie above the upper 90% limit, are ruled out. Next moment of inertia and quadrupole moment are calculated for merger component masses (1.58, 1.18) M_{\odot} . It follows from the calculation that the upper bounds on moments of inertia of merger components might be constrained in the range $\sim 1 - 2 \times 10^{45}$ g cm². As masses and moments of inertia are known, it is possible to estimate the radii of merger components which are ~ 13 km. The upper bounds on quadrupole moments of the merger components are found to be $0.29-0.3 \times 10^{43}$ g cm².

I. INTRODUCTION

The discovery of gravitational waves from the binary neutron star merger event GW170817 followed by the detection of its transient counterparts across the electromagnetic (EM) spectrum has heralded a new era in multimessenger astrophysics [1, 2]. The observed short Gamma Ray Burst (GRB) 1.7 s after the coalescence time provides clinching evidences for the association of short GRBs with neutron star mergers. This discovery of two colliding neutron stars and its aftermath led to plethora of information about short Gamma Ray Bursts, binary chirp mass, tidal deformability and dense matter in neutron star interior, speed of gravitational waves and heavy element synthesis due to r-process in ejected neutron-rich matter. The gravitational wave data led to the estimation of the binary chirp mass, $\mathcal{M}_{chirp} = (m_1 m_2)^{3/5} / (m_1 + m_2)^{1/5}$ in the 90% credible interval as $1.188^{+0.004}_{-0.002} M_\odot$ [1]. For low spin prior, the component masses of the binary lie in the range 1.17-1.6 M_\odot , whereas the total mass of the binary is $2.74^{+0.04}_{-0.01} M_\odot$. The binary mass ratio ($q = m_2/m_1$) is constrained in the range 0.7 - 1.0 for low spin prior. The optical/infrared transient several hours after GW170817 was found to be consistent with emissions of a Kilonova which shines through radioactive decays of r-process nuclei synthesised in the neutron-rich ejected matter [3, 4].

The observation of GW170817 reveals many interesting aspects of dense matter in neutron stars and its equation of state (EoS). The fate of the compact remnant formed in the binary neutron star merger might be closely related to the amount of ejected material as estimated from EM signals [5]. A prompt collapse is ruled out by the quantity of blue kilonova ejecta observed in optical wavelengths. It is argued that the merger remnant was born as a hypermassive neutron star (HMNS) supported by differential rotation for a short duration of time. This picture of short lived HMNS might be consistent with the large quantity of red Kilonova ejecta, as observed in the infrared, originating from the accretion torus around the HMNS before its collapse to a black hole. The compact remnant spined down emitting gravitational waves and might have collapsed to a black hole close to the mass-shedding limit of uniformly rotating neutron stars [6]. This conclusion about the merger remnant leads to the upper bound on the maximum mass of non-rotating neutron stars and much tighter constraint on the EoS of dense matter [5–8]. The lower bound on the maximum mass of neutron stars is obtained from pulsar observations.

It was long debated that the tidal effects in the late inspiralling phase of binary neutron

stars could be large and detected by gravitational wave detectors [9–11]. The tidal deformation of a neutron star might provide crucial information about the dense matter EoS. The effective tidal deformability parameter is expected to be determined from gravitational wave signals. Indeed this was achieved in GW170817. The LIGO and VIRGO observations of GW170817 placed an upper limit on the dimensionless combined tidal deformability $\bar{\Lambda} \leq 800$ in the low spin case at 90% confidence level [1]. A lower limit on $\bar{\Lambda} \geq 400$ was estimated from the observational data of the electromagnetic counterpart of GW170817 combined with numerical relativity simulations [7]. Recently another alternative approach involving radiative transfer simulations for the electromagnetic transient AT2017gfo predicts the lower bound on the tidal deformability to be $\bar{\Lambda} \geq 197$ [12].

The lower and upper bounds on the tidal deformability parameter put strong constraints on the dense matter EoS in neutron star interior. Radice et al. showed that too soft or too stiff EoSs were rejected because of those constraints [7]. Masses, radii and moments of inertia of neutron stars are the direct probes of dense matter EoS. The knowledge of tidal deformability from GW170817 was exploited to constrain the neutron star radius. It was shown that the upper limit of the radius of a $1.4 M_{\odot}$ neutron star was ≤ 13.76 km [13]. In another investigation with one million different EoSs, the radius (R) of a $1.4 M_{\odot}$ neutron star is found to be $12.00 \leq R/km \leq 13.45$ [14]. So far we have noticed that gravitational wave data from GW170817 as well as its EM counterpart AT2017gfo led to the determination of upper bounds on the mass and radius of non-rotating neutron stars. The question is whether the measured tidal deformability could put some bounds on the moments of inertia of merger components of GW170817. This motivates us to explore this problem in this work. This paper is organised in the following way. Equations of state used in this calculation are described in Sec II. We discuss results in Sec. III. We summarise our findings and conclude in Sec. IV.

II. FORMALISM

We discuss the computation of tidal deformability, moment of inertia and quadrupole moment in this section. These quantities are EoS dependent [15]. We adopt different relativistic mean field (RMF) models for the EoS of beta-equilibrated and charge neutral matter. The strong interaction among nucleons from the crust to the core is mediated

by the exchange of scalar, vector and iso-vector mesons in these RMF models. The RMF parametrizations used in this calculations are TM1, TMA, SFHo, SFHx, DD2, DDME2 [16, 17]. An extended nuclear statistical model developed by Hempel and Schaffner (HS) is used to describe the matter in the sub-saturation density regime [18] along with the RMF nuclear interactions for the nonuniform and high density matter in all these cases. The SFHo and SFHx EoSs are fitted to some measurements of neutron star radii [19]. The density dependent (DD) couplings are used in the RMF models of nuclear interactions denoted by DDME2 and DD2 [17, 20]. The DD2 RMF model is extended to include Λ hyperons involving repulsive interaction mediated due to ϕ mesons, by Banik, Hempel and Bandyopadhyay (BHB) and is denoted as BHB $\Lambda\phi$ [21]. All the above mentioned EoSs are unified in the sense that the same RMF model used in the crust and core. Furthermore, these EoS are widely used for core collapse supernova and neutron star merger simulations. We consider also equations of state involving first-order phase transition from hadronic matter to quark matter. In one case, the hadronic phase including all hyperons and Δ resonance are described by the DD2 RMF model [22]. For the quark phase made of u, d and s quarks, a non-local extension of the Nambu-Jona-Lasinio model is employed [23]. Gibbs phase rules are imposed in the hadron-quark (HQ) mixed phase. We label this EoS as HQ1. The hadronic phase in other HQ EoS made of only nucleons is calculated using the NL3 RMF model whereas the quark phase is described by the effective bag model including quark interaction [24]. The HQ mixed phase in this case is based on the Maxwell construction. This EoS is denoted as HQ2.

A static and spherically symmetric star develops a quadrupole moment (Q_{ij}) in response to a static external quadrupolar tidal field ϵ_{ij} . The tidal deformability in the linear order is defined as $\lambda = -\frac{Q_{ij}}{\epsilon_{ij}}$. The $l = 2$ dimensionless tidal Love number k_2 related to λ is given by [10]

$$\lambda = \frac{2}{3}k_2R^5 . \quad (1)$$

The spherically symmetric star under the linear $l = 2$, $m = 0$ perturbation due to the tidal field results in a static, even-parity perturbation of the metric which in the Regge-Wheeler gauge reduces to [10]

$$\begin{aligned}
ds^2 = & -e^{2\Phi(r)} [1 + H(r)Y_{20}(\theta, \varphi)] dt^2 \\
& + e^{2\Lambda(r)} [1 - H(r)Y_{20}(\theta, \varphi)] dr^2 \\
& + r^2 [1 - K(r)Y_{20}(\theta, \varphi)] (d\theta^2 + \sin^2 \theta d\varphi^2),
\end{aligned} \tag{2}$$

where, $K'(r) = H'(r) + 2H(r)\Phi'(r)$. Finally a second order differential equation for metric function H is obtained as

$$\begin{aligned}
H'' + H' \left(\frac{2}{r} + \Phi' - \Lambda' \right) + H \left(-\frac{6e^{2\Lambda}}{r^2} - 2(\Phi')^2 \right. \\
\left. + 2\Phi'' + \frac{3}{r}\Lambda' + \frac{7}{r}\Phi' - 2\Phi'\Lambda' + \frac{f}{r}(\Phi' + \Lambda') \right) = 0,
\end{aligned} \tag{3}$$

where, $f = d\epsilon/dp$. This equation is integrated outward from the center. Applying the asymptotic behaviour of $H(r)$, the $\ell = 2$ tidal love number is given by,

$$\begin{aligned}
k_2 = & \frac{8C^5}{5} (1 - 2C)^2 [2 + 2C(y - 1) - y] \\
& \times \left\{ 2C[6 - 3y + 3C(5y - 8)] \right. \\
& + 4C^3[13 - 11y + C(3y - 2) + 2C^2(1 + y)] \\
& \left. + 3(1 - 2C)^2 [2 - y + 2C(y - 1)] \ln(1 - 2C) \right\}^{-1},
\end{aligned} \tag{4}$$

$y = RH'(R)/H(R)$ and compactness of the star, $C = M/R$.

The dimensionless tidal deformability, dimensionless moment of inertia and dimensionless quadrupole moment are defined as $\Lambda_{1,2} = \frac{\lambda_{1,2}}{m_{1,2}^5}$, $\bar{I}_{1,2} = \frac{I_{1,2}}{m_{1,2}^3}$ and $\bar{Q}_{1,2} = \frac{Q_{1,2}}{(m_{1,2}^3(J_{1,2}/m_{1,2}^2)^2)}$ respectively, where subscripts 1 and 2 correspond to masses of merger components, m_1 and m_2 respectively. Quadrupole moment $Q_{1,2}$ is compared with the Kerr solution quadrupole moment $J_{1,2}^2/m_{1,2}$ and the dimensionless $\bar{Q}_{1,2}$ are known as Kerr factors corresponding to $m_{1,2}$. Moment of inertia and quadrupole moment are calculated by the spectral scheme within the numerical library LORENE [25, 26].

III. RESULTS AND DISCUSSION

We adopt nuclear EoSs HS(TM1), HS(TMA), HS(SFHo), HS(SFHx), DDME2, HS(DD2), hyperon EoS BHBA ϕ and hadron-quark EoSs HQ1 and HQ2 for the calculation of neutron

star properties as described in the section II. Figure 1 shows neutron star mass as a function of radius for the above mentioned EoSs. All those EoSs are compatible with $2 M_{\odot}$ neutron stars. We could learn valuable lessons about dense matter EoS from the fate of the massive remnant in GW170817. It is inferred that a hypermassive neutron star was born in the binary merger event and later it collapsed to a black hole. In this scenario, different groups estimated the upper bound on the maximum mass of non-rotating neutron stars (M_{max}^{TOV}) to be $2.16 M_{\odot}$ [5, 6, 8, 27]. On the other hand, the lower limit on the neutron star maximum mass $2.01 \pm 0.04 M_{\odot}$ was obtained from the observations of galactic neutron stars. Both bounds on the neutron star maximum mass i.e. $2.01 \pm 0.04 \leq M_{TOV}/M_{\odot} \leq 2.16 \pm 0.03$, put strong constraints on the EoS of dense matter. All EoSs except DD2, DDME2 and HS(TM1) satisfy these constraints on M_{max}^{TOV} as shown by two horizontal lines in Fig. 1.

Tidal deformability Λ_2 is plotted with Λ_1 in Fig. 2 for all those EoSs considered here. Dimensionless tidal deformabilities of both merger components are calculated using the same EoS. It also shows the 50% and 90% credible intervals (black solid and dashed lines) for the low spin case obtained using waveform models of TaylorF2 and PhenomPNRT [1, 28]. As the tidal deformability is directly proportional to R^5 , the compactness increases from top right corner to bottom left corner of Fig. 2. The SFHo EOS represents neutron stars with maximum compactness among all EOSs. The HQ2 EoS on the top right corner implies the least compact neutron stars and lies far outside the 90% credible interval. It is noted that HS(DD2) and BHBA ϕ EoSs which were allowed by TaylorF2 model, are now marginally compatible with the 90% contour of PhenomPNRT. The other EOSs which fall well inside 50% and 90% confidence intervals of PhenomPNRT are validated.

It has been argued that the tidal deformability parameter could probe the low density part of dense matter EoS. This can be understood very well from Figs. 1 and 2. The upper limit on neutron star maximum mass allows HQ2 and HS(TMA) along with several other EoSs as evident from Fig. 1. However, HQ2 and HS(TMA) EoSs are ruled out by the 90% confidence contour in Fig. 2. This demonstrates that the low density part of HQ2 and HS(TMA) essentially determines the tidal deformability. For example, the nuclear matter EoS in hadron-quark phase transition in HQ2 is described by the NL3 EoS which is very stiff. On the other hand, the neutron star maximum mass is estimated by the overall EoS which becomes softer due to the phase transition to quark matter.

Neutron star mass is plotted as a function of individual tidal deformability for BHBA ϕ

and SFHo EoSs in Fig. 3. The tidal deformability decreases as the neutron star becomes more massive. This also results in higher compactness. Consequently, more compact neutron stars will be less deformed. The tidal deformability for a $1.4 M_{\odot}$ neutron star is 697 and 334 in case of BHBA ϕ and SFHo EoSs, respectively.

LIGO and Virgo observations extracted the tidal contribution from the inspiral phase. The parameter ($\bar{\Lambda}$) that enters into the phase of the gravitational wave signal is a mass-weighted linear combination of individual dimensional tidal deformabilities as [29]

$$\bar{\Lambda} = \frac{16}{13} \frac{(m_1 + 12m_2)m_1^4\Lambda_1 + (m_2 + 12m_1)m_2^4\Lambda_2}{(m_1 + m_2)^5} \quad (5)$$

which is considered to be less than 720 at 90% confidence level [28] for low spin prior. Also an additional constraint is placed on $\bar{\Lambda} \geq 197$ is based on EM observations of GW170817 [12]. So the allowed window for $\bar{\Lambda}$ is now $197 \leq \bar{\Lambda} \leq 720$.

Mass weighted average tidal deformability parameter $\bar{\Lambda}$ is plotted with the ratio (q) of masses of merger components for a fixed chirp mass $\mathcal{M}_{chirp} = 1.188 M_{\odot}$ in case of low spin scenario in Fig. 4. Here results are shown for all EoSs. Upper and lower boundaries on $\bar{\Lambda}$ that were obtained from the gravitational wave and EM observations, respectively, are also shown in Fig. 4. It is found that results corresponding to all EoSs satisfy the lower boundary. However, this can not be said about several EoSs with respect to the upper boundary. It is evident from Fig. 4 that HS(DD2) and BHBA ϕ EoSs are marginally outside the upper boundary whereas HS(TM1), HS(TMA), HQ1 and HQ2 EoSs are conclusively ruled out by the GW data. It is worth mentioning here that the estimates of both boundaries are strongly model dependent [7, 12, 28].

We calculate gross properties such as moment of inertia and quadrupole moment of slowly rotating neutron stars with spin frequency 100 Hz in this calculation using LORENE. Figures 5 and 6 show the relations between the parameter $\bar{\Lambda}$ versus dimensionless moments of inertia of merger components \bar{I}_1 and \bar{I}_2 , respectively. These results are obtained for masses of merger components (m_1, m_2) are $(1.58, 1.18) M_{\odot}$ as calculated from the chirp mass. The upper bound on $\bar{\Lambda}$ is also included on the plot. The intersections of the curves with the upper bound of $\bar{\Lambda}$ as obtained from gravitational wave data of GW170817 give upper limits on the values of moments of inertia of two merger components. The values of I_1 and I_2 so obtained are $\sim 2.0 \times 10^{45}$ g/cm² and $\sim 1.2 \times 10^{45}$ g/cm², respectively. These values of moments of inertia are consistent with the theoretically predicted values of Ref.[30].

As we know the moment of inertia and mass of each component, it is possible to estimate the radius of the corresponding component. This is done using the universal relation between dimensionless moment of inertia and compactness of neutron star [31]. This universal relation is shown in Fig. 7 for equations of state considered here except HQ EoSs in Fig. 7. The universal relation is fitted with the functional form as given by Eq. (20) of Ref. [31]. It is evident that the upper limit on the tidal deformability constrains radii of merger components to ~ 13 km which are independent of component masses [32]. It is worth mentioning here that HQ EoSs violate the universality [33].

We do the similar investigation for quadrupole moments (Q_1, Q_2) of merger components in GW170817. Figures 8 and 9 exhibit the behaviour of mass weighted average tidal deformability parameter with dimensionless quadrupole moments \bar{Q}_1 and \bar{Q}_2 , respectively. The upper limit on $\bar{\Lambda}$ from gravitational wave observation of GW170817 is also shown in both figures. The values of upper bounds on quadrupole moments lie in the range 0.29 - 0.30 $\times 10^{43}$ g cm². Unlike the cases of moments of inertia in Figs. 5 and 6, the estimated value of upper bound on Q_1 is less than that of Q_2 because the latter merger component is less compact and it is easy to deform the star.

IV. CONCLUSION

We investigate properties of merger components of GW170817 particularly moment of inertia and quadrupole moment of slowly rotating neutron stars using the LORENE. We exploit large number of different EoSs involving nucleons, hyperons and quarks. Next we compute the mass weighted average tidal deformability parameter, moment of inertia and quadrupole moment of merger components using the same EoS. All those quantities are dependent on EOS. We find that 50 % and 90 % credible intervals on the mass weighted average tidal deformability parameter $\bar{\Lambda}$ obtained from gravitational wave data of GW170817 allow soft to moderately stiff EoSs. BHBA ϕ EoS might be marginally allowed by 90% credible interval whereas too stiff EoS like HS(TM1), HS(TMA) and HQ2 are ruled out. Next we obtain upper bounds on moments of inertia and quadrupole moments exploiting the upper limit on the parameter $\bar{\Lambda}$ due to gravitational wave observation of GW170817. These estimates are the first of its kind. It is possible to determine radii of two merger

components when masses and moments of inertia of two merger components are known.

- [1] B. P. Abbott et al., *Phys. Rev. Lett.* **119**, 161101 (2017).
- [2] B. P. Abbott et al., *Astrophys. J. Lett.* **848**, L13 (2017).
- [3] B. D. Metzger, *Living Rev. Relativity* **20**, 3 (2017).
- [4] B. D. Metzger et al., *Mon. Not. R. Soc.* **406**, 2650 (2010).
- [5] B. Margalit and B. D. Metzger, *Astrophys. J. Lett.* **850**, L19 (2017).
- [6] L. Rezzolla, E. R. Most and L. R. Weith, *Astrophys. J. Lett.* **852**, L25 (2018).
- [7] D. Radice, A. Perego, F. Zappa and S. Bernuzzi, *Astrophys. J. Lett.* **852**, L29 (2018).
- [8] M. Ruiz, S. L. Shapiro and A. Tsokaros, *Phys. Rev. D* **97**, 021501 (2018).
- [9] E. E. Flanagan and T. Hinderer, *Phys. Rev. D* **77**, 021502 (2008).
- [10] T. Hinderer, *Astrophys. J.* **677**, 1216 (2008).
- [11] T. Hinderer, B. D. Lackey, R. N. Lang and J.S. Read, *Phys. Rev. D* **81**, 1230161 (2010).
- [12] M. W. Coughlin et al., arXiv:1805.09371.
- [13] F. J. Fattoyev, J. Piekarewicz and C. J. Horowitz, *Phys. Rev. Lett.* **120**, 172702 (2018).
- [14] E. R. Most and L. R. Weith, L. Rezzolla and J. Schaffner-Bielich, arXiv:**1803.00549**.
- [15] D. Bandyopadhyay, S.A. Bhat, P. Char and D. Chatterjee, *Eur. Phys. J. A* **54**, 26 (2018).
- [16] M. Oertel, M. Hempel, T. Klähn, and S. Typel, *Rev. Mod. Phys.* **89**, 015007 (2017).
- [17] G. A. Lallazissis, T. Niksić, D. Vretenar and P. Ring, *Phys. Rev. C* **71**, 024312 (2005).
- [18] M. Hempel and J. Schaffner-Bielich, *Nucl. Phys. A* **837**, 210 (2010).
- [19] A. W. Steiner, M. Hempel and T. Fischer, *Astrophys. J.* **774**, 17 (2013).
- [20] S. Typel et al., *Phys. Rev. C* **81**, 015803 (2010).
- [21] S. Banik, M. Hempel and D. Bandyopadhyay, *ApJS* **214**, 22 (2014).
- [22] R. D. Mellinger Jr, F. Weber, W. Spinella, G. A. Contrera and M. G. Orsaria, *Universe*, **3**, 1 (2017).
- [23] M. Orsaria, H. Rodrigues, F. Weber and G. A. Contrera, *Phys. Rev. D*, **87**, 023001 (2013).
- [24] I. N. Mishustin, R. Mallick, R. Nandi and L. Satarov, *Phys. Rev. C*, **91**, 055806 (2015).
- [25] E. Gourgoulhon, P. Grandclément, J.-A. Marck, J. Novak and K. Taniguchi, "LORENE spectral methods differential equation solver", *Astrophysics Source Code Library ascl:1608.018*, (2016).

- [26] <http://www.lorene.obspm.fr/>
- [27] S. Banik and D. Bandyopadhyay, **arXiv:1712.09760**.
- [28] B. P. Abbott et al., **arXiv:1805.11579**.
- [29] M. Fatava, Phys. Rev. Lett., **112**, 101101 (2014).
- [30] S. Bhattacharyya, I. Bombaci, D. Bandyopadhyay, A. V. Thampan and D. Logoteyta, New Astronomy, **54**, 61 (2017).
- [31] C. Breu and L. Rezzolla, Mon. Not. R. Astron. Soc. **459** 646 (2016).
- [32] C. Raithel, F. Özel and D. Psaltis, **arXiv:1803.07687**.
- [33] D. Bandyopadhyay, S. A. Bhat, P. Char and D. Chatterjee, Eur. Phys. J. A, **54**, 26 (2018).

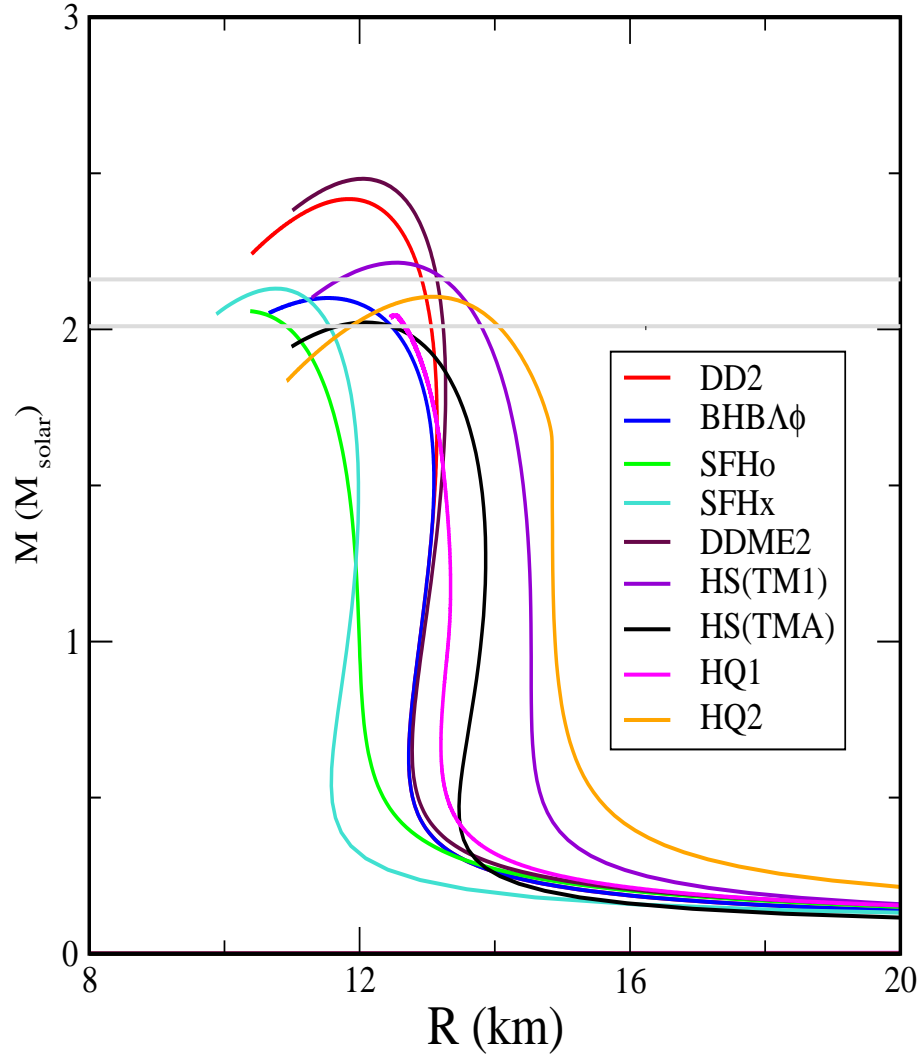


Fig. 1. Mass-radius relation is plotted for different equations of state.

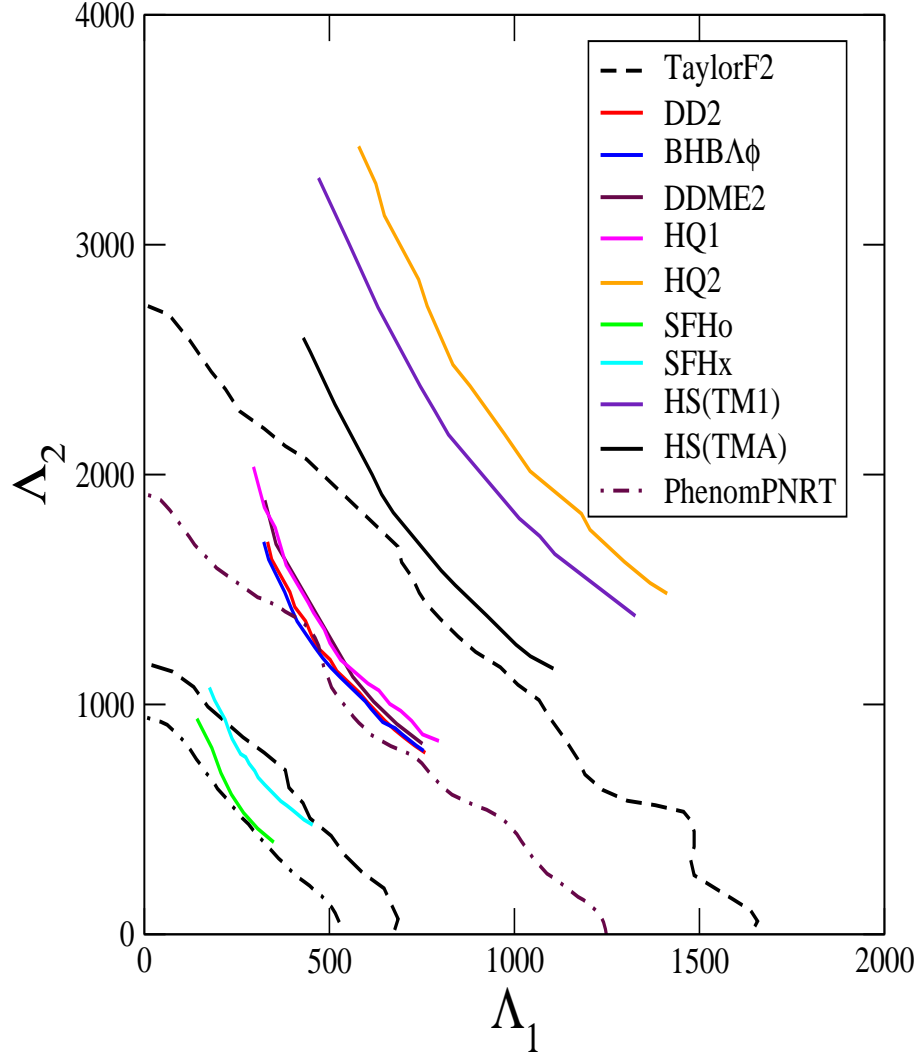


Fig. 2. Dimensionless tidal deformability parameters Λ_1 and Λ_2 are plotted here for different equations of state. Dashed and dashed dot lines denote the 50 % and 90 % probability contours as obtained from Ref.[1, 28].

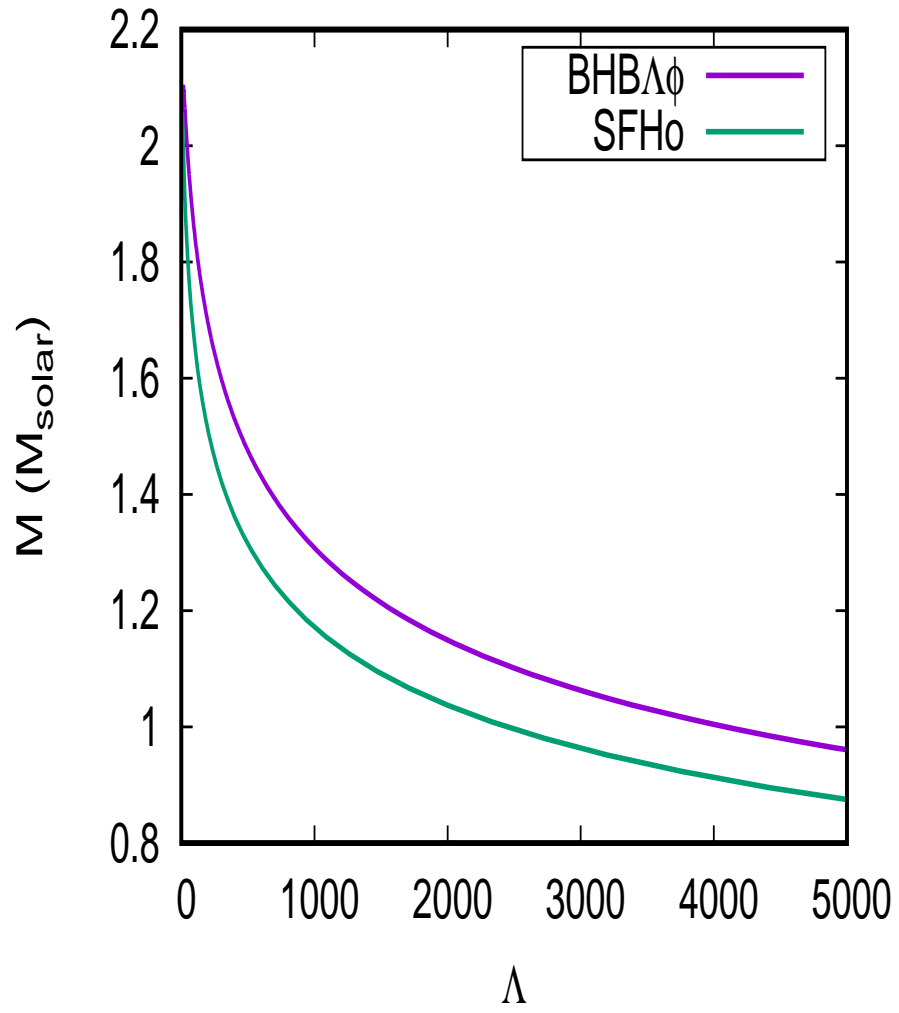


Fig. 3. Mass of neutron star is plotted as a function of tidal deformability for BHBAΦ and SFHo equations of state.

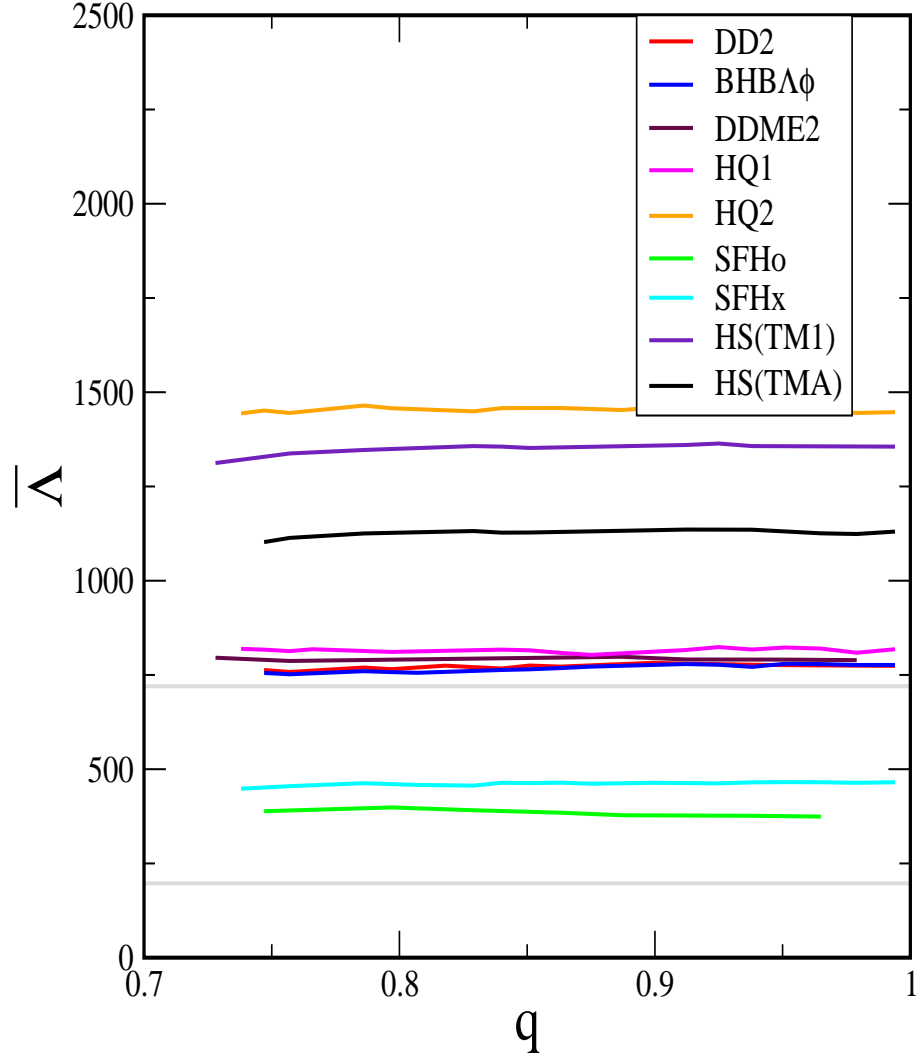


Fig. 4. Tidal parameter $\bar{\Lambda}$ is plotted against mass ratio q for a fixed chirp mass $\mathcal{M}_{chirp} = 1.188 M_{solar}$. Observational upper and lower limits are shown here.

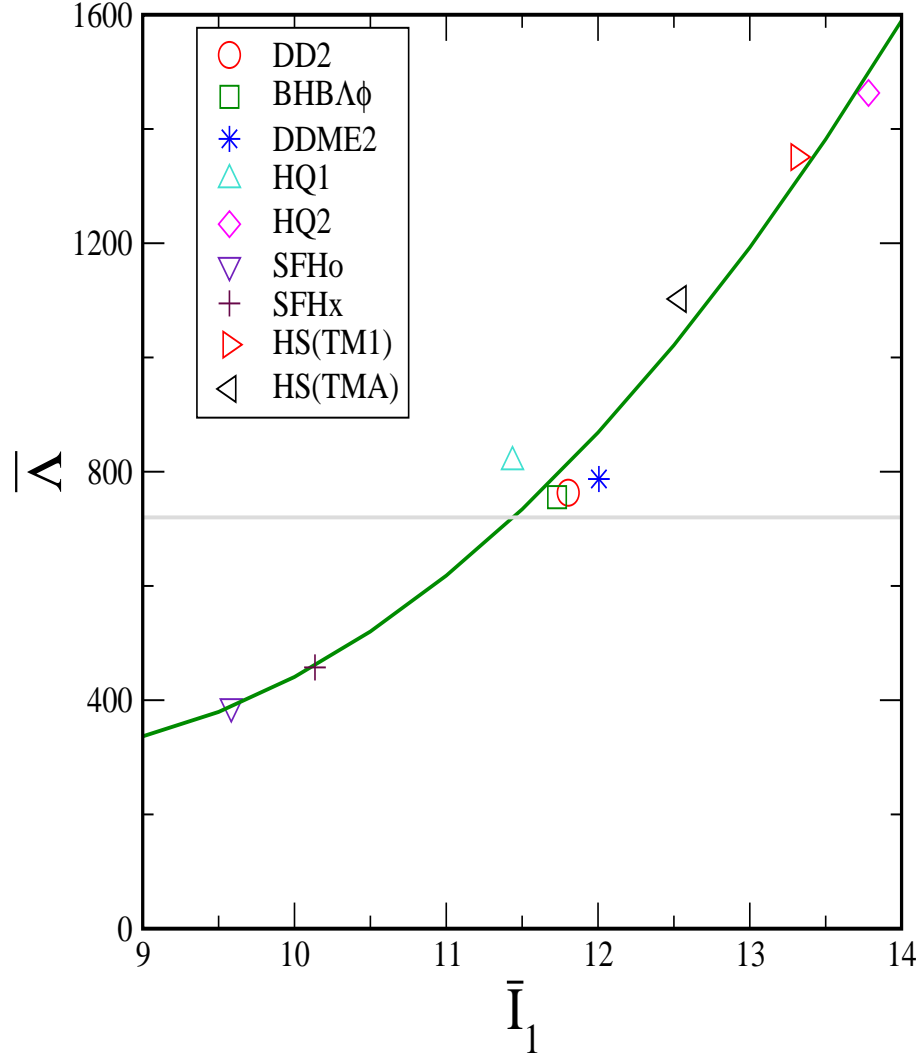


Fig. 5. Mass weighted average tidal deformability parameter $\bar{\Lambda}$ is shown as a function of dimensionless moment of inertia of the heavier component of the neutron star binary having mass $1.58 M_{\odot}$.

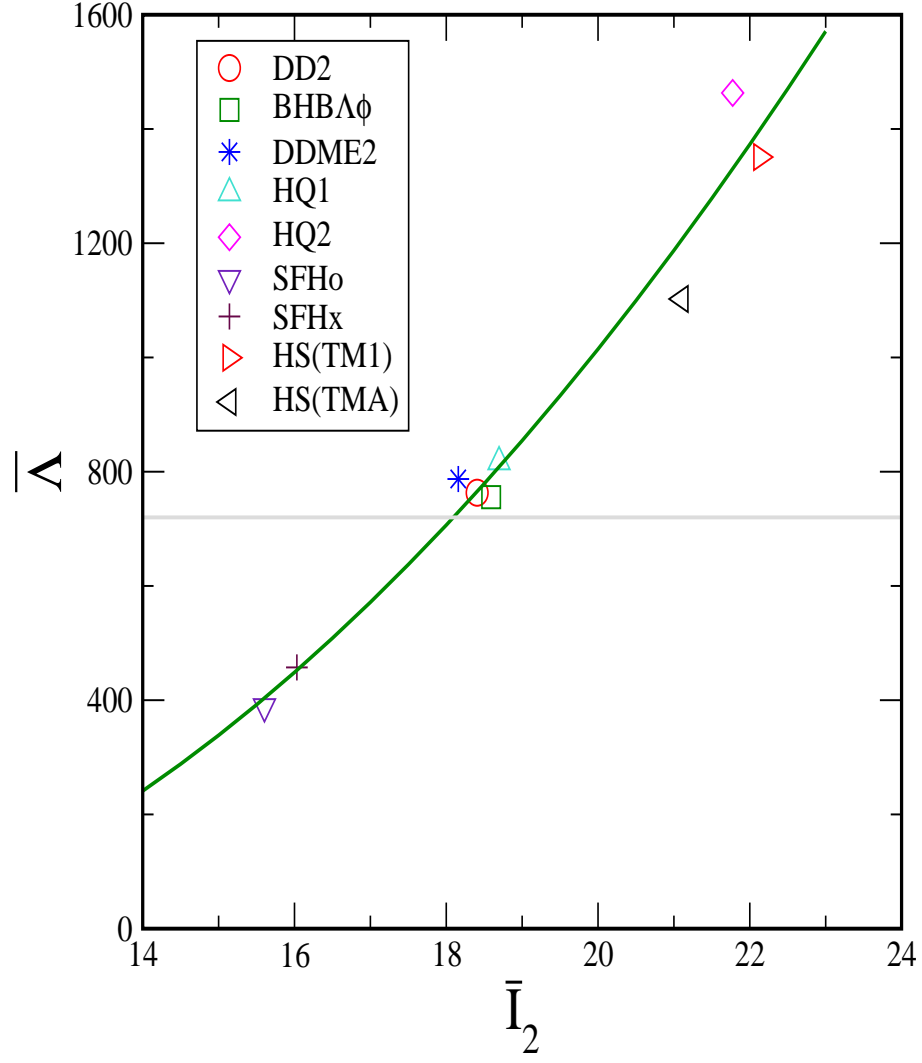


Fig. 6. Same as Fig. 4, but for the lighter component of the neutron star binary having mass $1.18 M_{\odot}$.

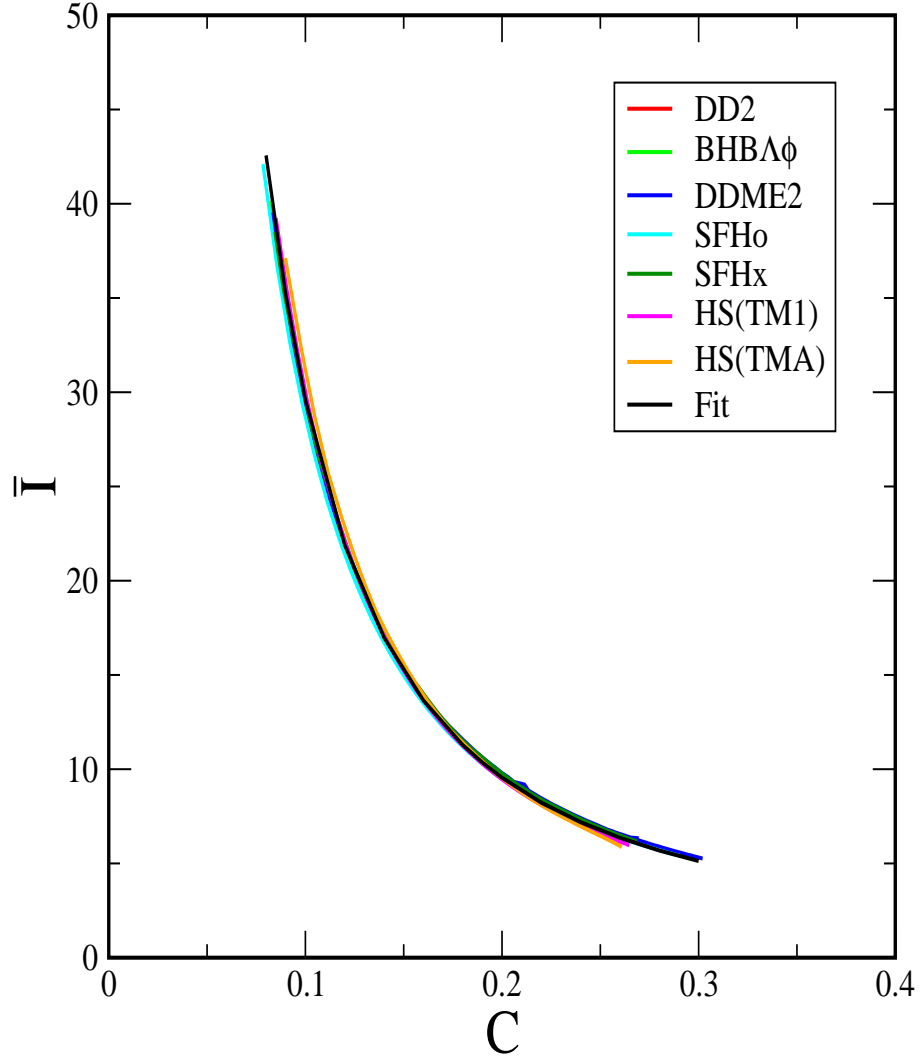


Fig. 7. Dimensionless moment of inertia is plotted with compactness of neutron star for different hadronic equations of state.

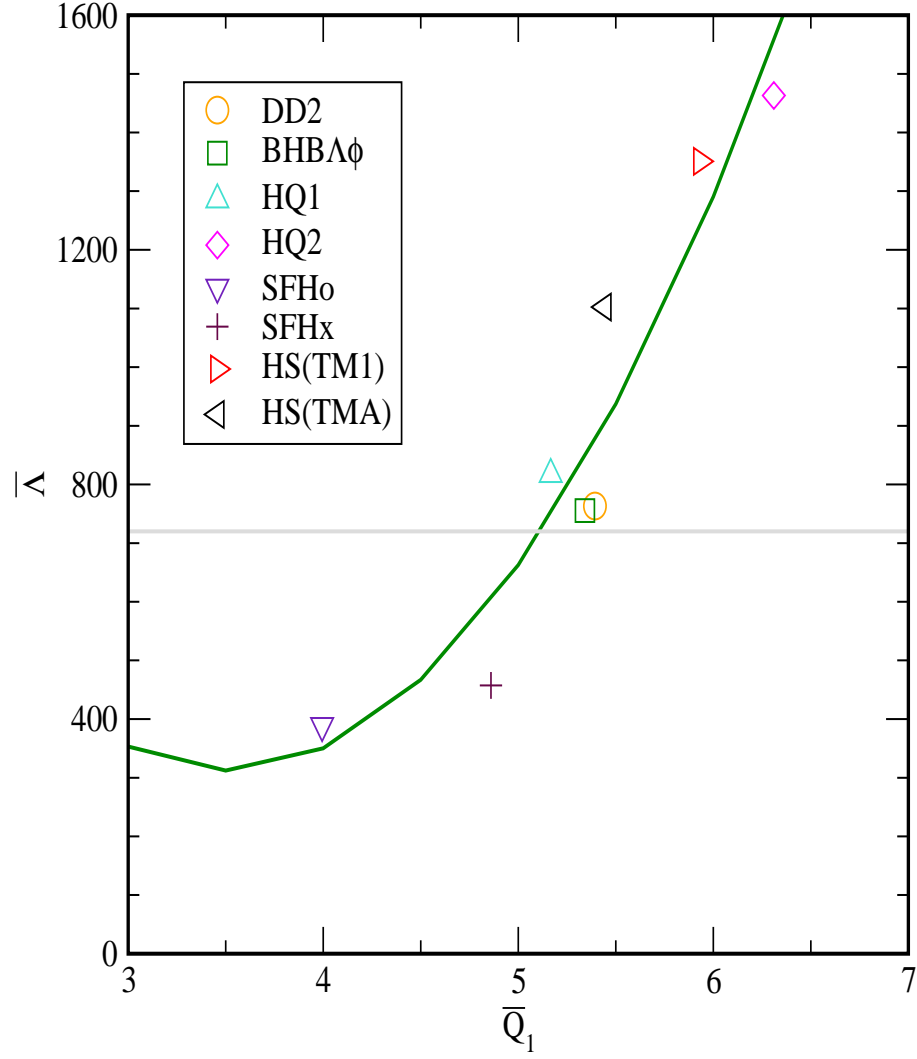


Fig. 8. Mass weighted average tidal deformability parameter ($\bar{\Lambda}$) is shown as a function of dimensionless quadrupole moment of the heavier component .

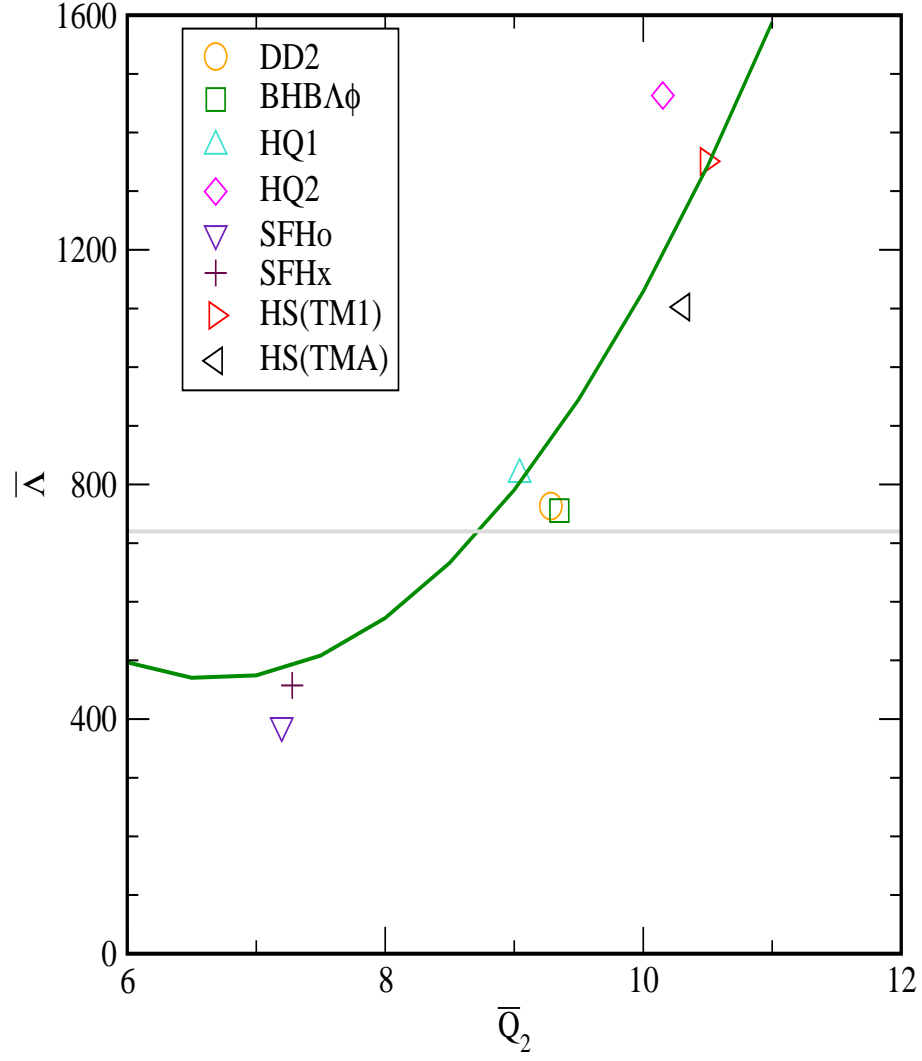


Fig. 9. Same as Fig. 6, but for the lighter component in the neutron star binary.